Supporting Information

A Bio-inspired Electrolyte with In-situ Repair of Zn Surface Crack and Regulation of Zn ion Solvation Chemistry to Enable Long-life and Deep-cycling Zinc Metal Batteries

Nan Hu[a], Wensong Lv[a], Huan Tang[b], Hongyu Qin[a], Yuhang Zhou[a], Li Yi[a], Dan Huang[b], Zhenrui Wu[c], Jian Liu[c], Zhengjun Chen[a], Jing Xu[a], Huibing He[a]**

[a]School of Chemistry and Chemical Engineering, Guangxi Key Laboratory of Petrochemical Resource Processing and Process Intensification Technology, Guangxi University, Nanning 530004, PR China

[b]School of Physical Science and Technology, Guangxi Novel Battery Materials Research Center of Engineering Technology, Guangxi University, Nanning 530004, PR China

[c]School of Engineering, Faculty of Applied Science, The University of British Columbia, Kelowna, BC V1V 1V7 Canada.

E-mail: huibinghe@gxu.edu.cn

Experimental Procedures

Preparation of Electrolyte: Zinc sulfate ($ZnSO_4 \cdot 7H_2O$, Guangdong guanghua, ≥99.5%), was dissolved into the deionized water (DI water) to obtain the 2 M $ZnSO_4$ basic electrolyte (BE). TEOS ($C_8H_{20}O_4Si$, Hushi, AR) with various concentration (5, 10, 20, 50 mm) was added into the as-prepared 2 M $ZnSO_4$ basic electrolyte to obtain the experimental sample. The optimized concentration (20 Mm) was used as DE. Zn@ZSO/BE was denoted as 2 M $ZnSO_4$ basic electrolyte and Zn foil soaked in DE.

Preparation of V_2O_5: Vanadium oxide (V_2O_5, Macklin, 99%, 0.3 g) was dissolved into 10 mL 2 M sodium chloride (NaCl) aqueous solution, after continuous stirring for 72 h, the forming orange red gel was sequentially washed with DI water and ethanol for several times. Then the product was dried at 80 °C in the vacuum oven for 12 h.

Preparation of cathode and anode: The V_2O_5 cathode was prepared by a slurry coating method, which was composed of commercial V_2O_5 powder, Super P, and polyvinylidene fluoride (PVDF) with mass ratio of 7:2:1 mixing in N-methyl-2-pyrrolidine (NMP). Then, the slurry pasted onto a Ti foil and vacuum-dried at 80 ºC overnight. The active loading mass for the V_2O_5 cathode was about 9.69 mg cm^{-2} (2.9 mA h cm^{-2}) and 3.31 mg cm^{-2} (0.99 mA h cm^{-2}). Zn/V_2O_5 full cell tests were assembled using ultrathin Zn electrodes (10 μm, 5.85 mA h cm^{-2}, 100 μm, 58.5 mA h cm^{-2}) as anode, V_2O_5 as cathode, and glass fiber as separator; and Zn or Cu electrodes with 100 μm thickness were used in the Zn|Zn and Cu|Zn cells.

Materials Characterizations: X-ray diffraction (XRD) patterns were carried out on a D/Max-III X-ray diffractometer (Rigaku Co., Japan) with Cu Kα radiation (λ = 0.15406 nm). Scanning electron microscopy (SEM) images and elemental mapping analysis (EDS) were obtained on a Sigma 300 (Zeiss, Germany). X-ray photoelectron spectroscopy (XPS) was performed on Thermo Scientific K-Alpha (Thermo Fisher Scientific, USA). The in-situ optical images were collected on a DMM-900C

metallographic microscope (Caikon optical instrument Co., Shanghai) by using an optical electrochemical cell (Hefei in-situ Technology Co., Ltd). Attenuated total reflection flourier transformed infrared spectroscopy (ATR-FTIR) was conducted on the Nicolet 670 (USA). NMR spectrum was performed using Bruker 600 M. Raman spectroscopy was performed using DXR 2Xi.

Electrochemical Measurements: CR2025 coin cells were assembled in the air to evaluate electrochemical performance. The cathode material of V_2O_5 was mixed with super P and polyvinylidene difluoride (PVDF) with a weight ratio of 7:2:1 by using N-methyl-2-pyrrolidone (NMP) as solvent. The slurry was then cast onto a Cu foil (thickness: 30 μm) by the doctor blade method and then dried under a vacuum at 60 °C overnight. After that, the electrode was cut into round disks (Φ = 10 mm) as the cathode in Zn/V_2O_5 full cells. The mass loading of active material is about 2.55 mg cm^{-2}. All galvanostatic measurements were carried out on a homo thermal NEWARE battery tester (MIHW-200-160CH, Shenzhen) at 25 °C. The electrochemical tests were all tested on an electrochemical workstation (Interface 1010E, Gamry, USA). Cyclic voltammetry (CV) of the Zn|Cu asymmetric cells was conducted in a voltage range of -0.2 to 2 V with a scan rate of 1 mV s^{-1}, which Cu foil served as the counter and reference electrode. For Zn/V_2O_5 full cells, CV was tested in the voltage range of 0.4 to 1.6 V (*vs.* Zn^{2+}/Zn) at a scan rate of 0.1 mV s^{-1}. Chronoamperometry (CA) curves were conducted at a constant overpotential of -150 mV for 500 s. Electrochemical Impedance Spectroscopy (EIS) was conducted in a frequency range of 100 kHz to 0.01 Hz with AC amplitude of 10 mV. The corrosion Tafel plots and the hydrogen evolution performance were both tested by the liner scan voltammetry (LSV) method in the three electrode system, which Zn foil, Pt plate, and Ag/AgCl act as working electrode, counter electrode, and reference electrode, respectively. The potential range of the corrosion Tafel plots was between -0.7 and -1.3 V (*vs.* open-circuit voltage) at a scan rate of 1 mV s^{-1} in 2 M $ZnSO_4$ solution, and the potential range of the hydrogen evolution performance was -0.9 to -1.6 V (*vs.* Ag/AgCl) at a scan rate of 1 mV s^{-1}. The surface area of the working electrode was 1 (1 × 1) cm^2. All the electrochemical testing

was conducted at the temperature of 25 °C. DEMS was performed on Hiden Analytical Ltd. HPR-40 with a sealed cell containing Zn electrodes (150 um thickness), glass fiber separator (GF/F, Whatman), and stainless-steel spacers (1 mm). Before testing, the system was deflated with pure He for 24 hours (0.5 mL min^{-1}) and reached ultra-high vacuum. Zn symmetric cell was cycled using a current of 2 mA cm^{-2} for 5 mAh cm^{-2}, and the resulting gases species (m/z=2 for H_2) was analyzed using DEMS. The depth of discharge (DOD) was calculated via the following equation:

$$DOD = \frac{3.6XM}{\rho N_A nel} \times 100\%$$

where X represents the capacity in each half cycle during the charge/discharge process, M represents the relative molecular mass of Zn (65.38 g mol^{-1}), ρ represents the zinc density (7.14 g cm^{-3}), N_A represents the Avogadro constant (6.02×10^{23} mol^{-1}), n represents the number of charge transfer of Zn^0 to Zn^{2+} (2), e represents the electric quantity of a charge (1.6×10^{-19} C) and l represents the thickness of Zn foil (0.01 cm).

Computational Details: The Density Functional Theory (DFT) calculations was implemented by Vienna *ab initio* simulation package (VASP).[1] The generalized gradient approximation function proposed by Perdew, Burke, and Ernzerhof (GGA-PBE)[2] was used to describe the exchange-correlation potential energy. The plane wave basis sets with projector-augmented wave (PAW) pseudopotentials were applied in calculations[3]. Van der Waals interaction was included in all calculations based on DFT-D3 grimme method.[4] The convergence tolerance of optimization was set as 1.0 × 10^{-4} eV for energy, and all the forces on each atom were smaller than 0.03 eV $Å^{-1}$. The plane-wave cutoff energy was set to 400 eV, and the Brillouin zone sampling was carried out on Gamma point. The Zn (002) slab is built with an 8 × 8 supercell, where the Zn substrate has four layers of atoms and the bottom two layers are fixed. A vacuum of 15 Å along the c axis was used to avoid interactions between layers. The adsorption energies (E_{abs}) of Zn surface with TEOS molecules, Free H_2O molecules respectively,

as well as Zn with TEOS molecules, Zn (002) surface, H_4SiO_4 molecules, SiO_2 molecules and Zn_xSiO_y molecules, respectively, which were calculated as:

$$E_{abs} = E_{total} - E_{molecule} - E_{Zn}$$

where E_{total}, $E_{molecule}$ and E_{Zn} are the total energy of the optimized adsorbate on Zn surface, the energy of the adsorbate, and the energy of Zn (002) surface or Zn, respectively.

[1] S. Grimme, J. Antony, S. Ehrlich, H. Krieg, *J Chem Phys,* 2010, **132**, 154104.

[2] S. Grimme, S. Ehrlich, L. Goerigk, *J Comput Chem,* 2011, **32**, 1456-1465.

[3] P. E. Blochl, *Phys Rev B Condens Matter,* 1994, **50**, 17953-17979.

[4] J. P. Perdew, K. Burke, M. Ernzerhof, *Physical Review Lett.,* 1996, **77**, 3865-3868.

Results and Discussion

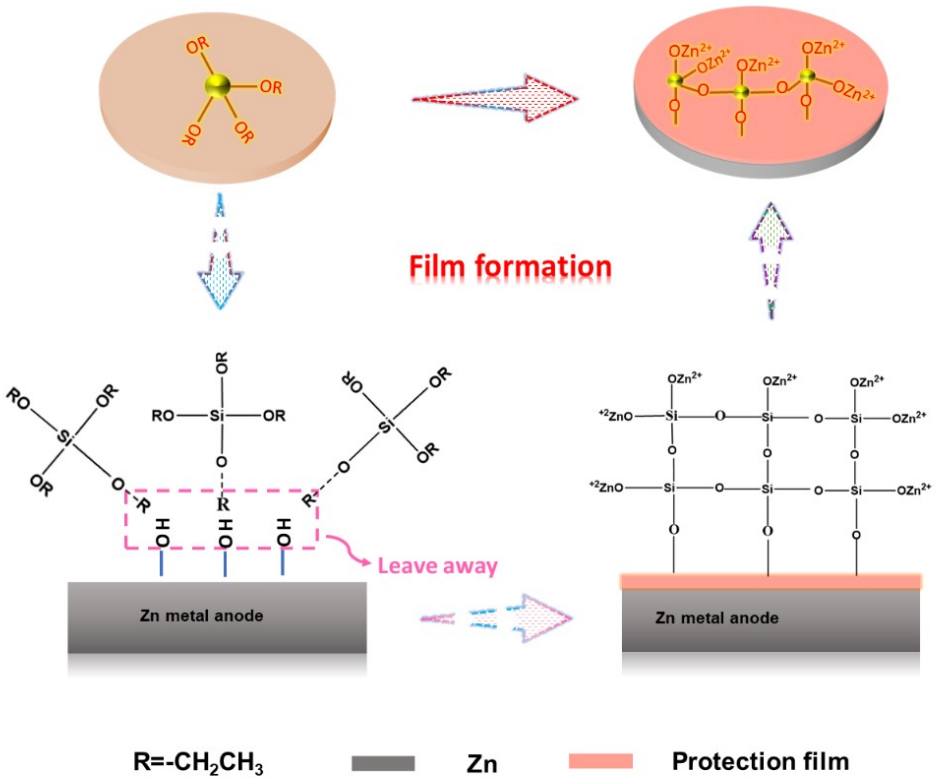

Figure S1. Schematic illustration of the ZSO protective film formation mechanism in DE.

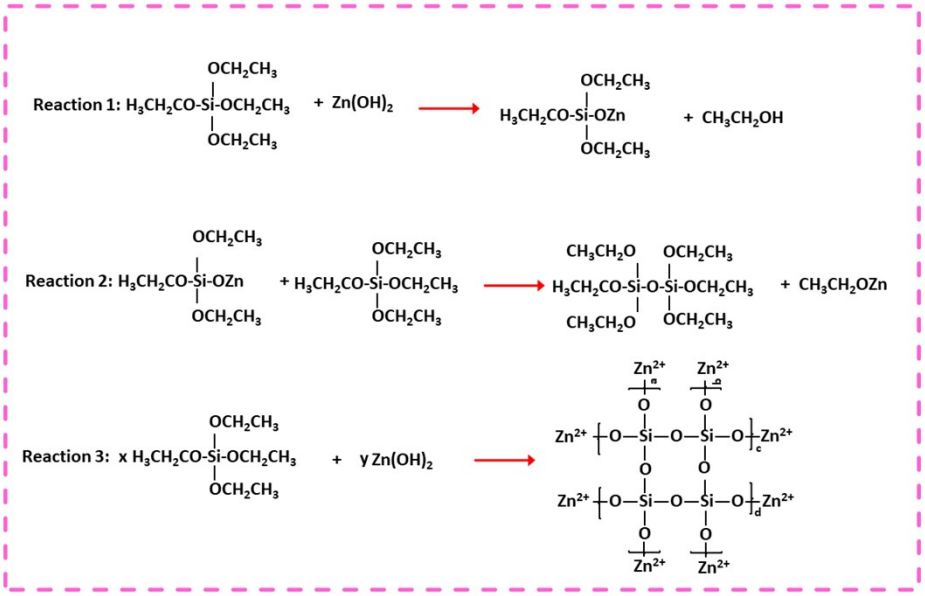

Figure S2. The possible reaction mechanism of the protective film formation.

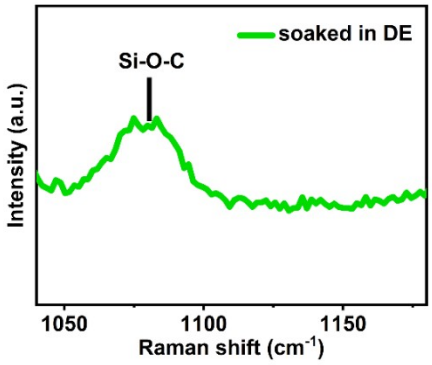

Figure S3. Raman spectrum of the Zn foil after soaking into DE.

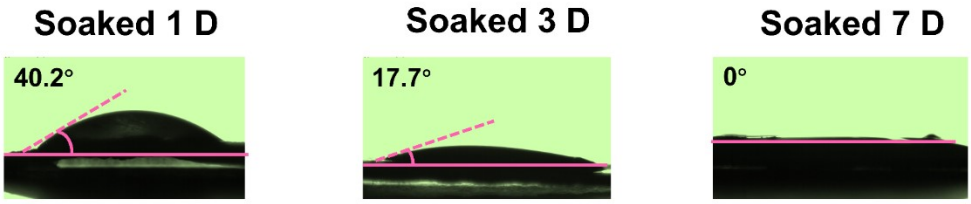

Figure S4. Contact angle measurements of the DE on the Zn electrode after soaking for 1, 3, 7 days.

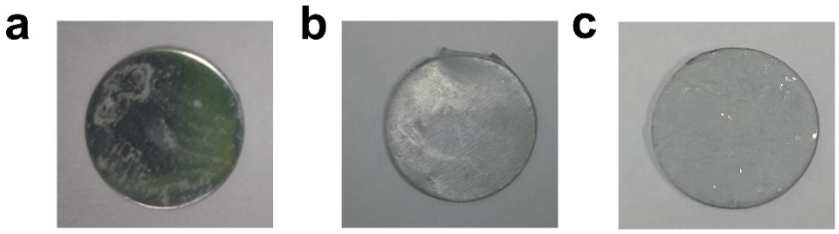

Figure S5. Optical images of the Zn anode after soaking for 1,3,7 days in DE.

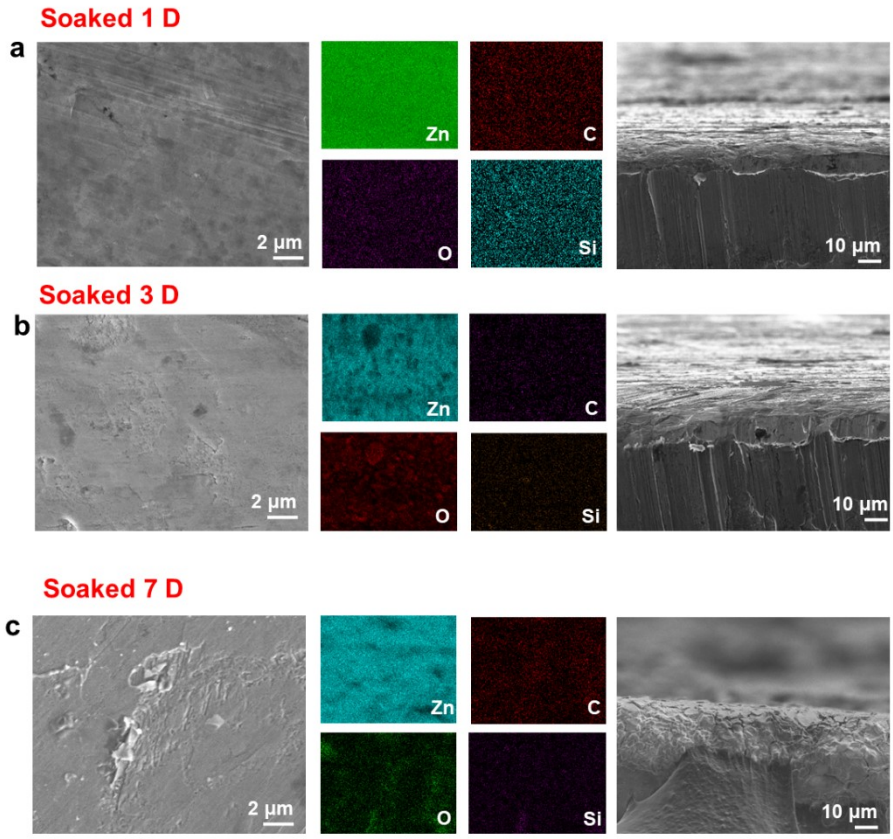

Figure S6. SEM image (side-view and top-view) and corresponding EDS mapping images of Zn, C, O and Si elements in the Zn anode after soaked for (a) 1 day, (b) 3 days and (c) 7 days in DE.

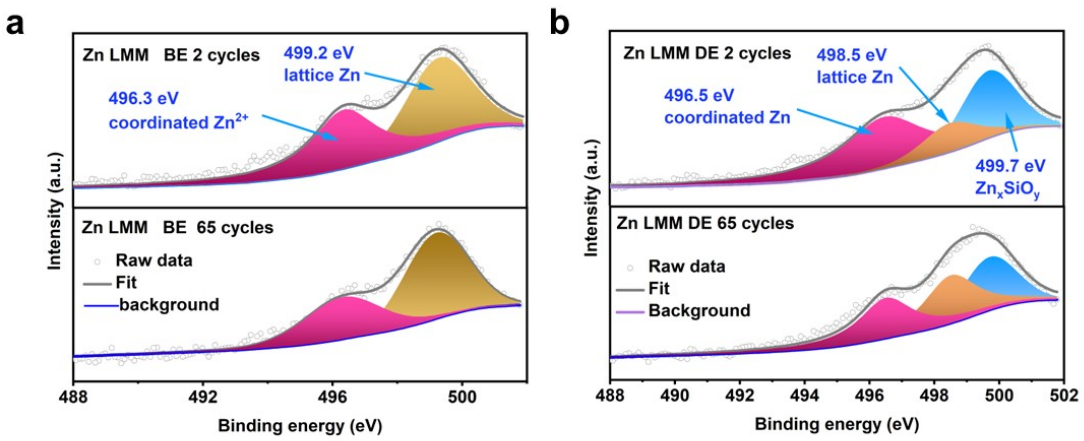

Figure S7. Zn LMM spectrum of the Zn anode after 2 cycles and 65 cycles in the DE and BE.

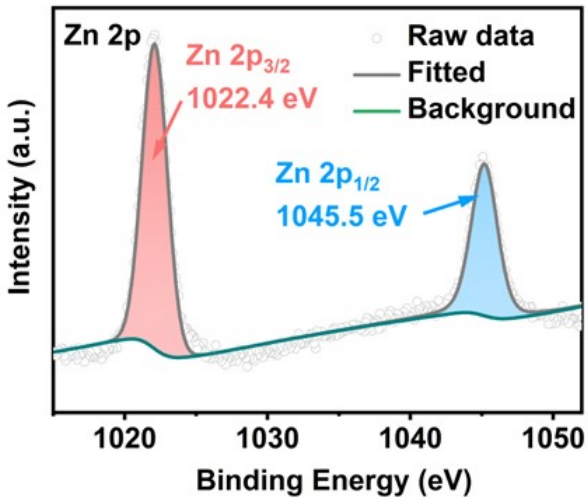

Figure S8. The full Zn 2p spectrum of the Zn anode after 65 cycles in DE.

Figure S9. Zn 2p XPS spectra of the Zn anode in BE after 2 cycles and 65 cycles.

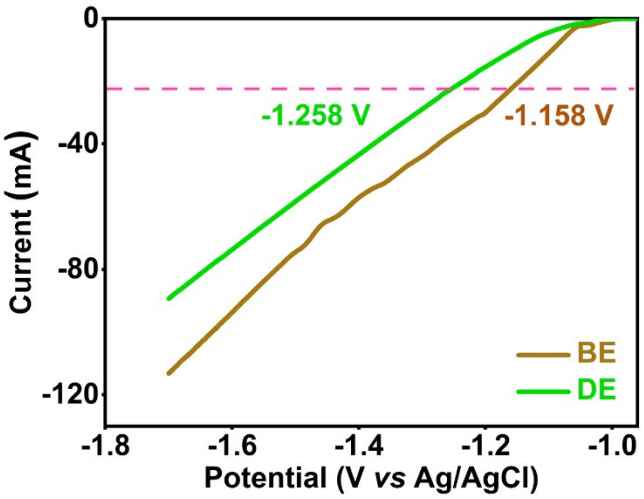

Figure S10. Linear polarization curves of the Zn anode in DE and BE.

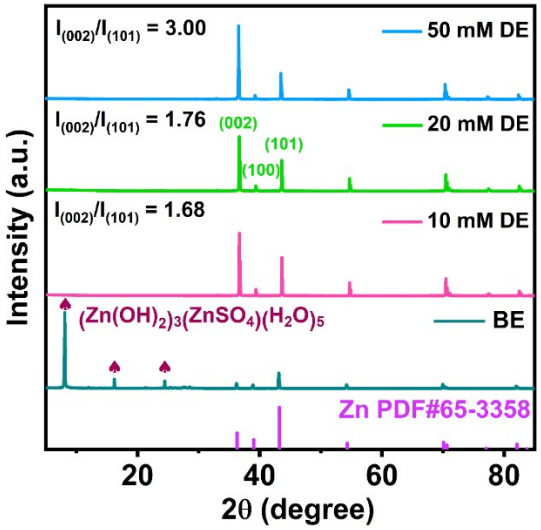

Figure S11. The XRD patterns of Zn anode cycled in DE of different concentrations.

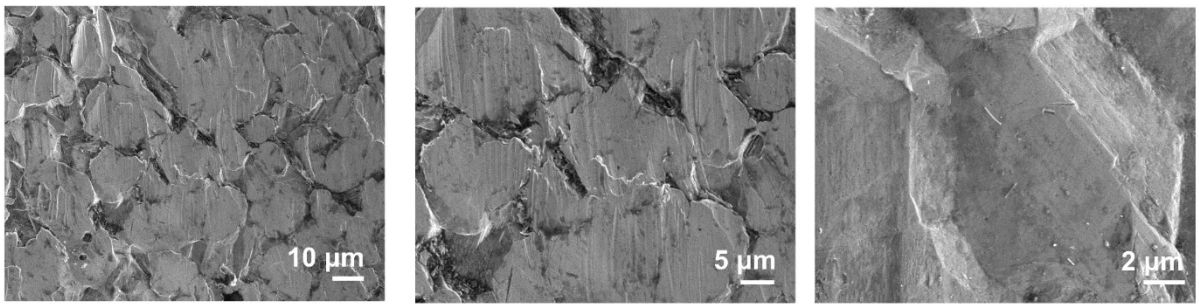

Figure S12. SEM images of Zn anode after 200 cycles in symmetrical Zn cells with 20 mM DE**.**

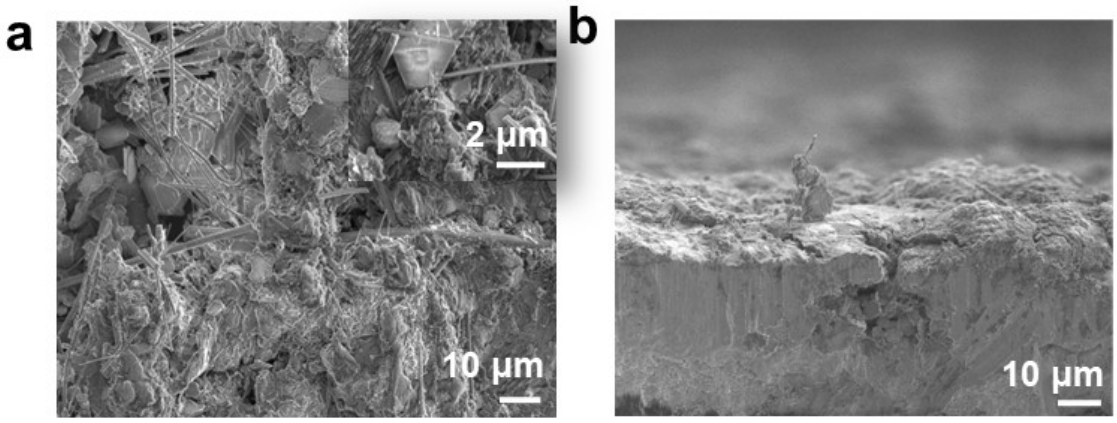

Figure S13. SEM images (a: top-view and b: side-view) of the Zn anode after 65 cycles at 0.5 mA cm^{-2} with a capacity of 0.5 mAh cm^{-2} in BE in other ratio bars.

Figure S14. SEM images (a: top-view and b: side-view) of the Zn anode after 65 cycles at 0.5 mA cm^{-2} with a capacity of 0.5 mAh cm^{-2} in DE in other ratio bars.

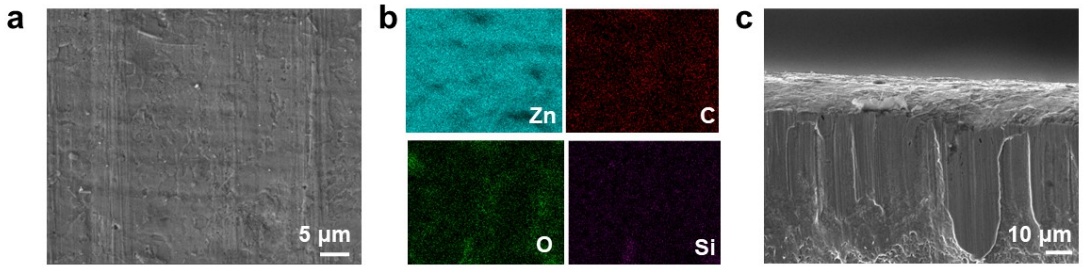

Figure S15. SEM images (a: top-view and c: side-view) of the Zn anode after 150 cycles at 0.5 mA cm^{-2} with a capacity of 0.5 mAh cm^{-2} in DE and the corresponding EDS of Zn, C, O, Si (b).

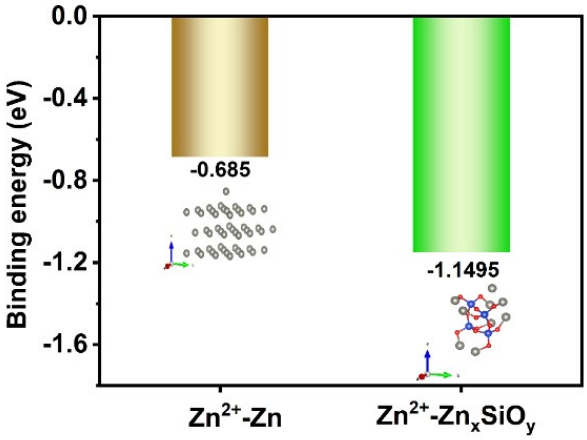

Figure S16. Calculated binding energies of Zn^{2+}-Zn, Zn^{2+}- Zn_xSiO_y and corresponding structures.

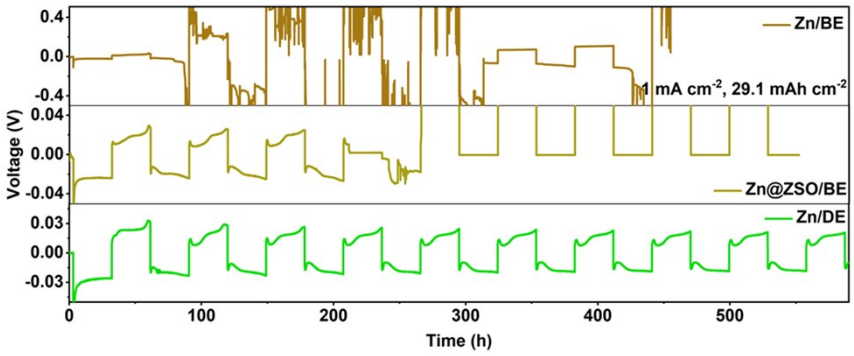

Figure S17. Galvanostatic voltage profiles of the Zn|Zn symmetric cell cycled in BE, Zn@ZSO|Zn@ZSO symmetric cell cycled in BE, and Zn|Zn symmetric cell cycled in DE at 1 mA cm^{-2}, 29.1 mAh cm^{-2} (DOD: 50%).

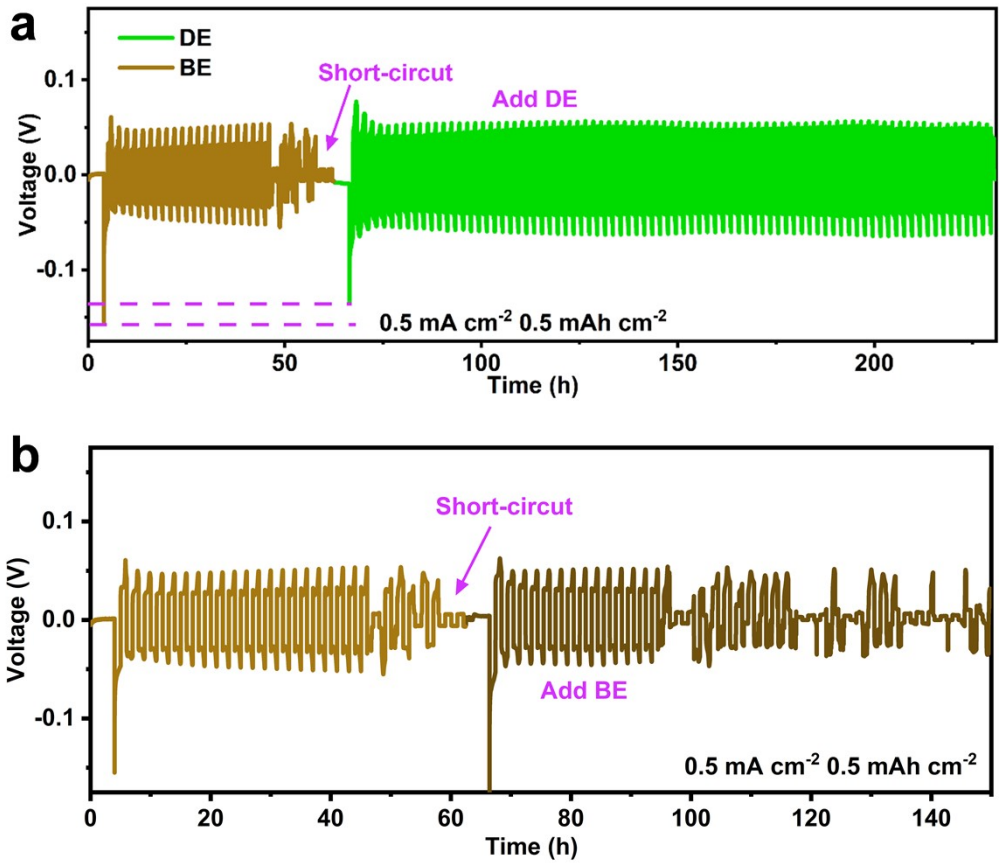

Figure S18. Galvanostatic voltage profiles of a Zn//Zn symmetric cell cycled in BE and changing to (a) DE (b) fresh BE for plating/stripping 0.5 mAh cm^{-2} at current densities of 0.5 mA cm^{-2}.

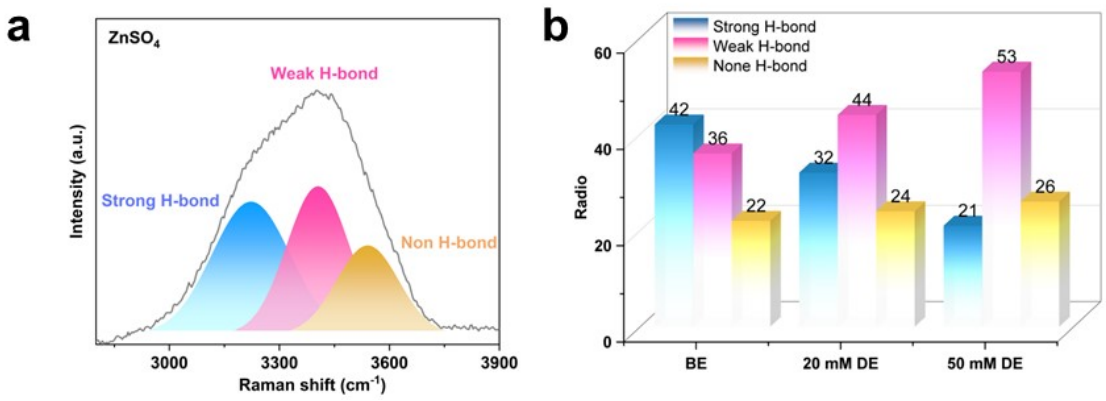

Figure S19. (a) the fitted Raman spectrum of water in BE and (b) the O–H stretching vibration fitted results of Raman spectra of the water molecules in BE, 20 mM DE, and 50 mM DE, respectively.

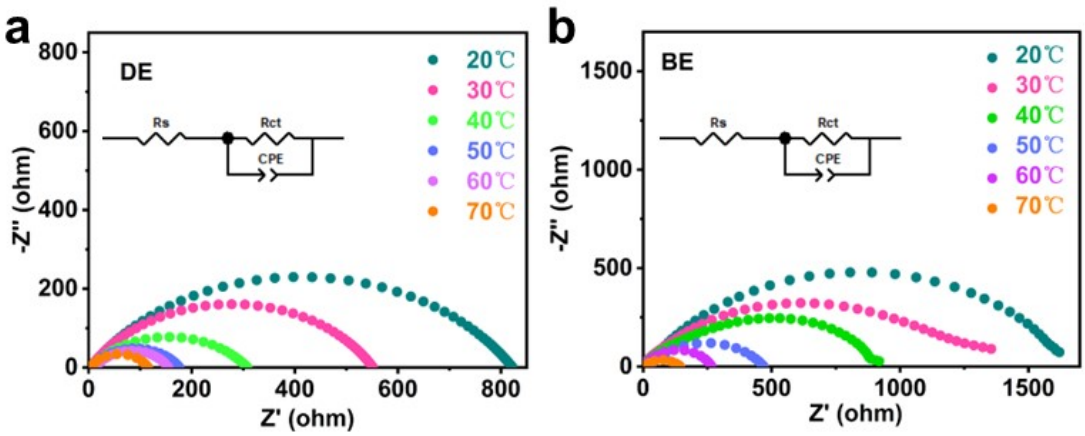

Figure S20. The EIS of Zn/Zn symmetrical cells using DE (a) or BE (b) at different temperature.

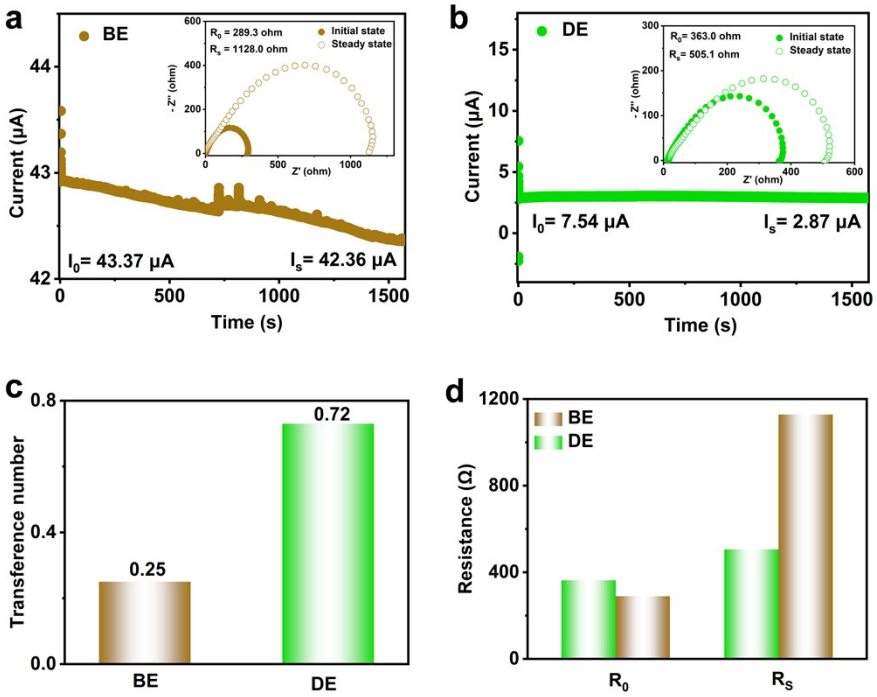

Figure S21. Current-time plots of Zn symmetric cell in (a) BE and (b) DE following polarization at a constant potential (25 mV) for 1500 s. The insets are the impedance spectra before and after the polarization. (c) The histogram of Zn^{2+} transference number in different electrolytes. (d) The histogram of R_0 and R_s in different electrolytes.

The transference number of Zn^{2+} (tZn^{2+}) was determined from:

$$tZn^{2+} = I_s\,(\Delta V - I_0R_0)/I_0\,(\Delta V - I_SR_S)$$

Where ΔV is the applied voltage (25 mV); I_0 and R_0 are the initial current and resistance, respectively; I_S and R_S are the steady-state current and resistance, respectively.

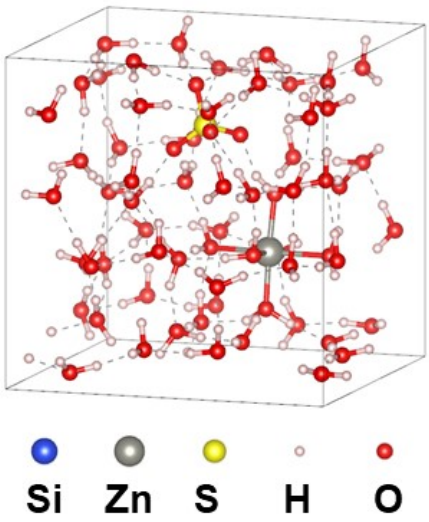

Figure S22. 3D snapshot of 2 M $ZnSO_4$ electrolyte (BE) system obtained from AIMD simulations.

Figure S23. RDFs for Zn^{2+}-O (H_2O) and the coordination number.

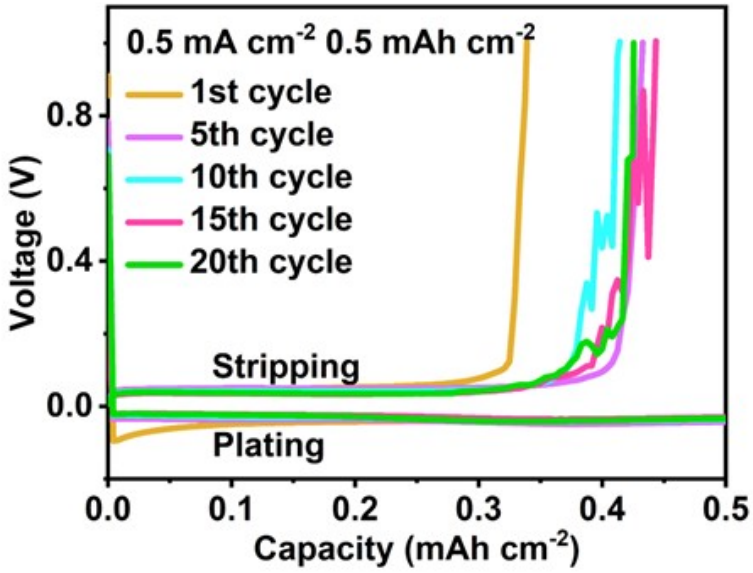

Figure S24. The corresponding voltage-capacity curves for the selected cycles in BE at 0.5 mA cm^{-2} with a capacity of 0.5 mAh cm^{-2}.

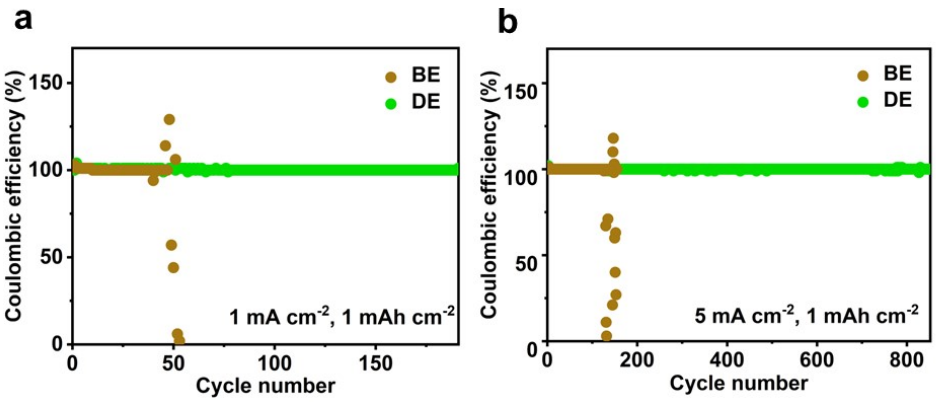

Figure S25. Coulombic efficiency of Cu|Zn cells at (a)1 mA cm^{-2} and (b) 5 mA cm^{-2} with the capacity of 1 mAh cm^{-2}.

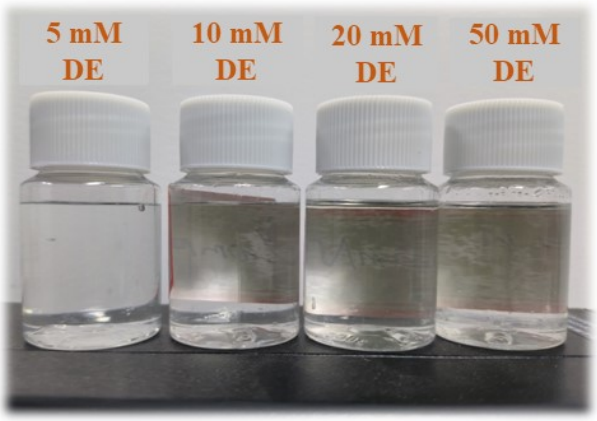

Figure S26. Optical images of the DE with different concentrations of 5, 10, 20 and 50 mM.

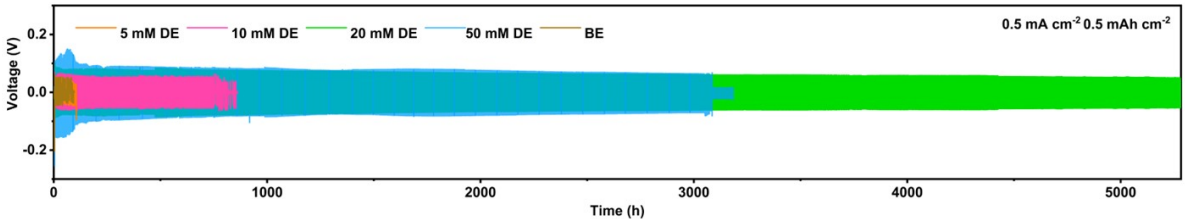

Figure S27. Comparison of the cycling stability of Zn|Zn symmetric cells tested in 2 M $ZnSO_4$ with DE of different concentrations at 0.5 mA cm^{-2}, 0.5 mAh cm^{-2}.

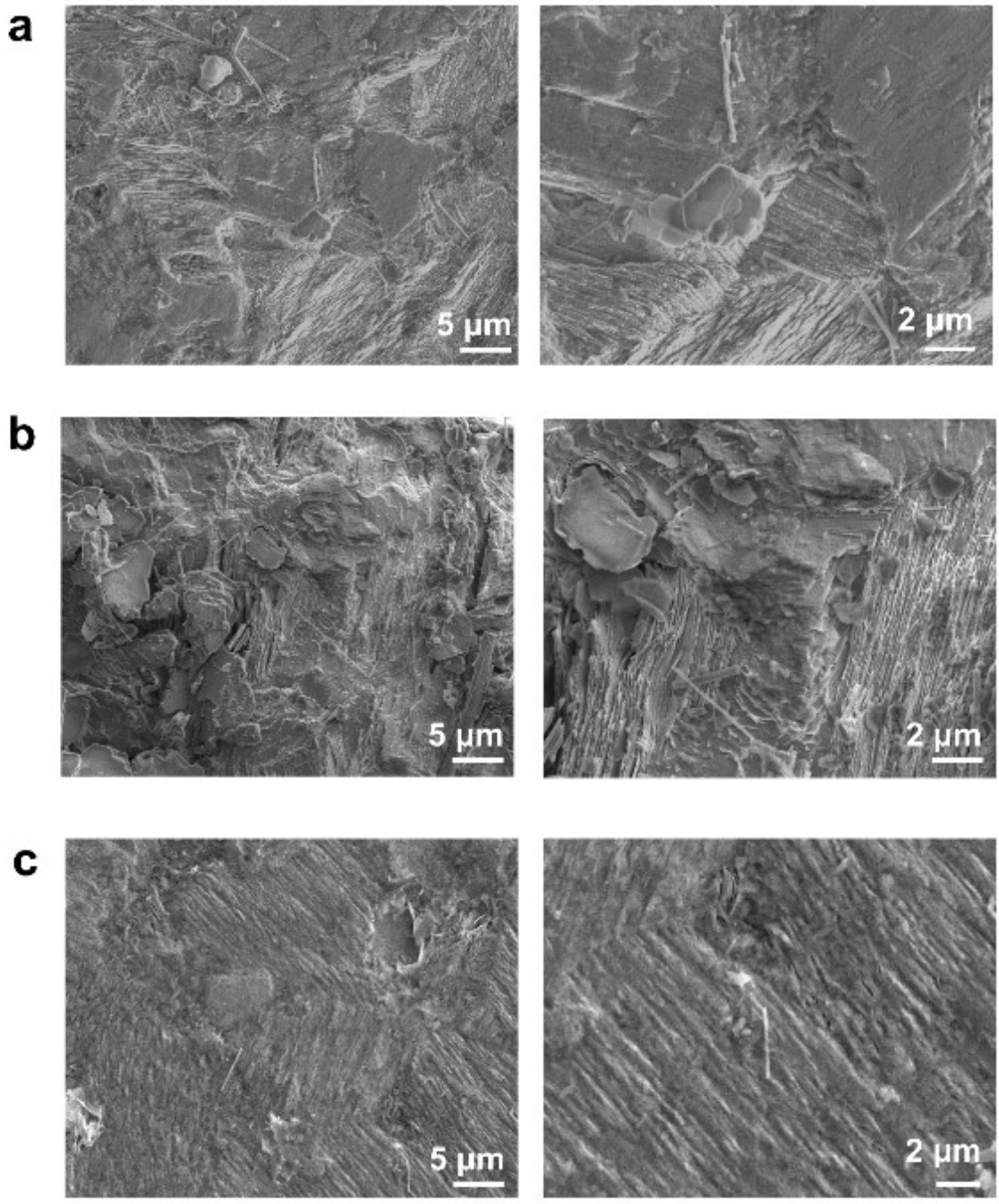

Figure S28. SEM images (top-view) of Zn deposits grown at Zn anode cycled in DE of (a) 5 mM (b) 10 mM and (c) 50 mM at 0.5 mA cm^{-2}, 0.5 mAh cm^{-2}.

Figure S29. CE of Zn|Cu cells in a series of DE at 0.5 mA cm^{-2}, 0.5 mAh cm^{-2}.

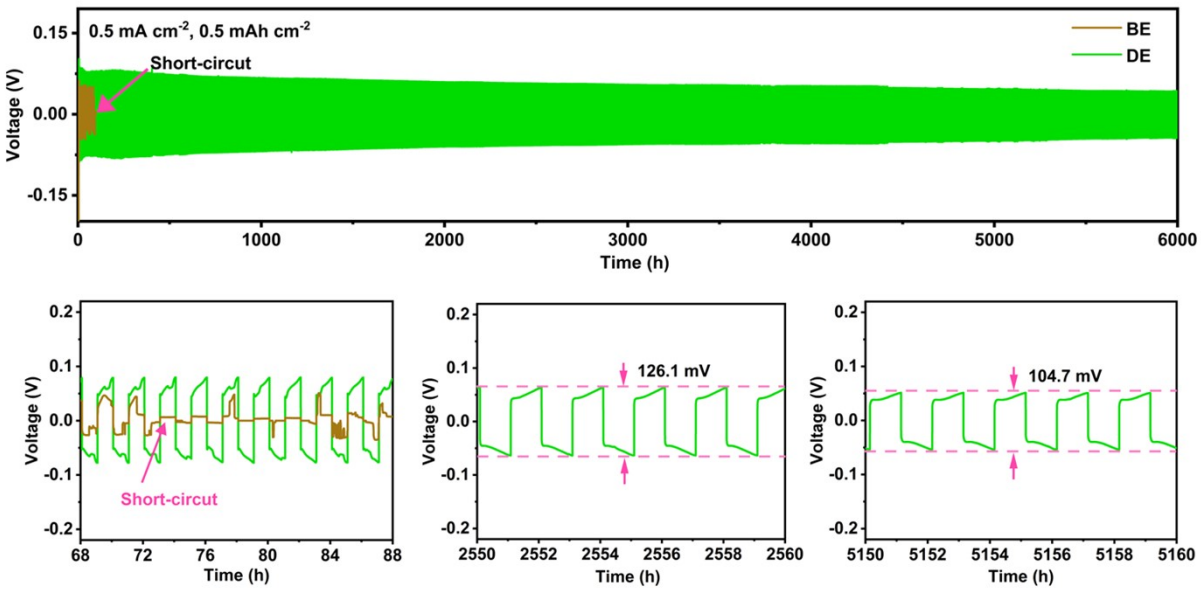

Figure S30. Cycling performance of the Zn|Zn symmetric cells at 0.5 mA cm^{-2}, 0.5 mAh cm^{-2} and polarization curves at different cycles.

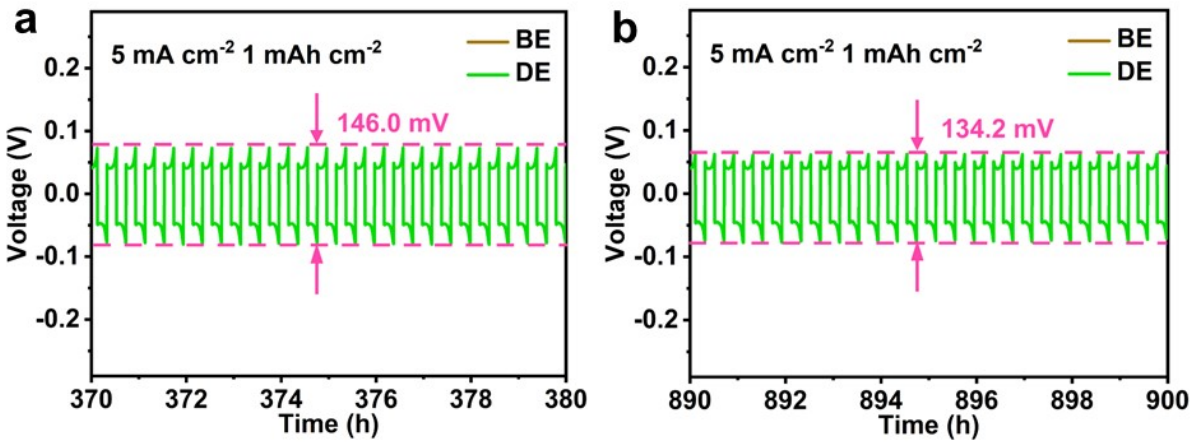

Figure S31. The enlarged polarization curves of different cycles at 5 mA cm^{-2},1 mAh cm^{-2}.

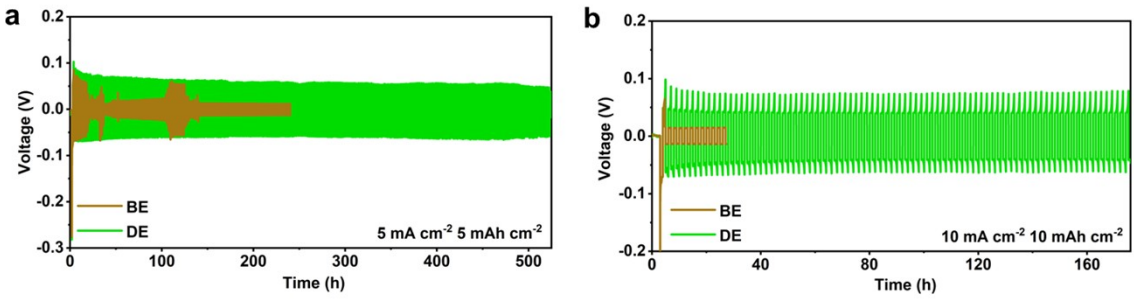

Figure S32. The electrochemical performance of the Zn|Zn symmetric cells at **(a)** 5 mA cm^{-2}, 5 mAh cm^{-2}, and (b) 10 mA cm^{-2}, 10 mAh cm^{-2}.

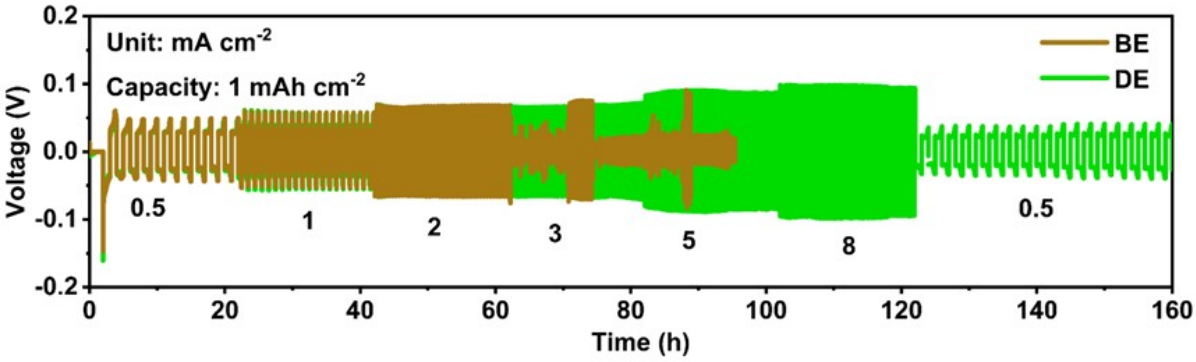

Figure S33. Rate performance of Zn|Zn symmetric cells in BE and DE at a spectrum of current densities (0.5, 1, 2, 3, 5, and 8 mA cm^{-2}) with a fixed areal capacity of 1 mAh cm^{-2}.

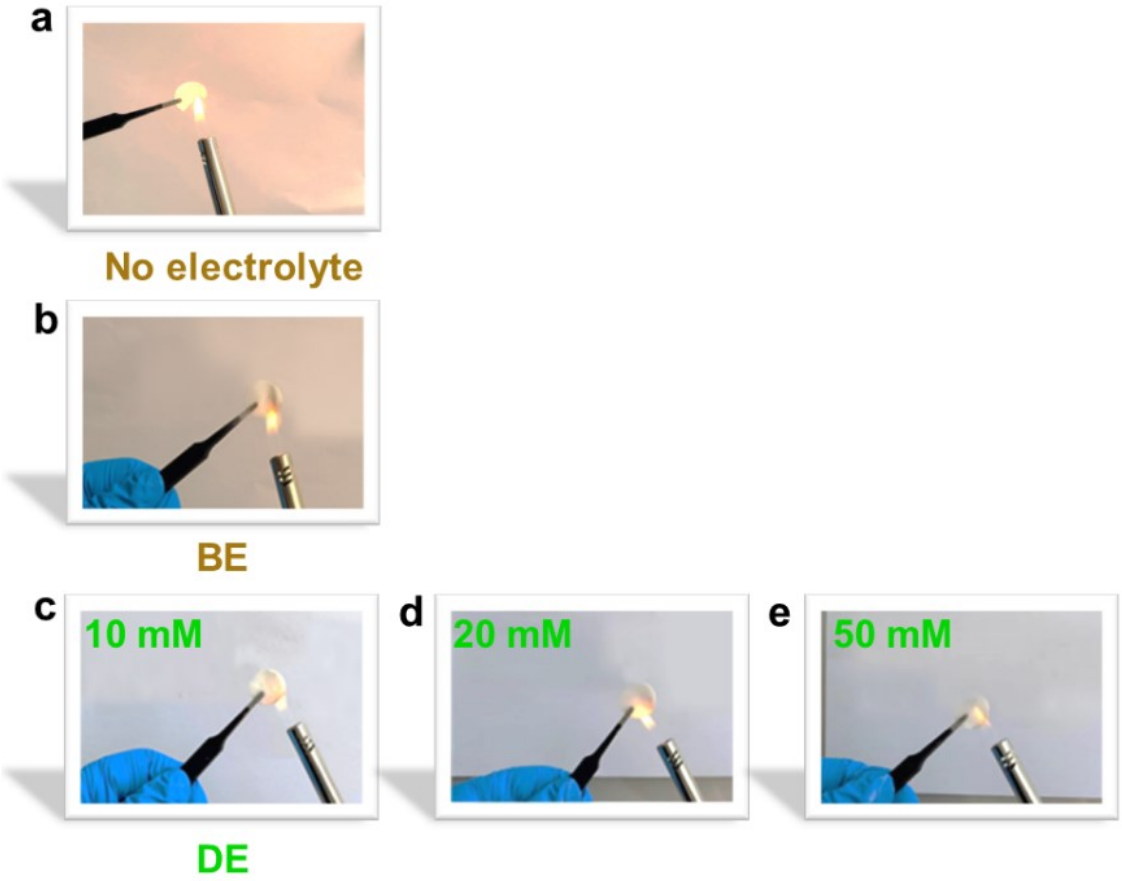

Figure S34. Photographs of the ignition test of (a) the glass fiber and (b) the BE, (c) 10 mM DE, (d) 20 mM DE, (e) 50 mM DE

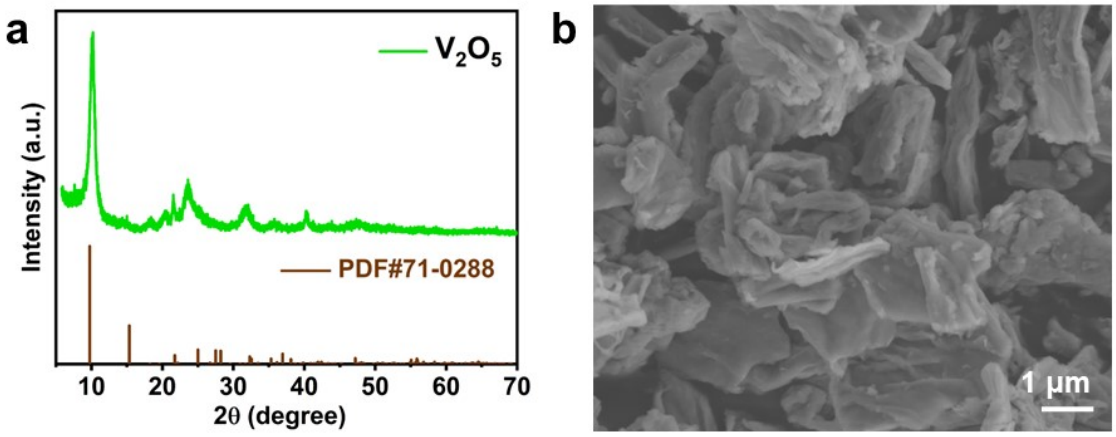

Figure S35. XRD pattern (a) and SEM image (b) of the synthesized V_2O_5 cathode materials.

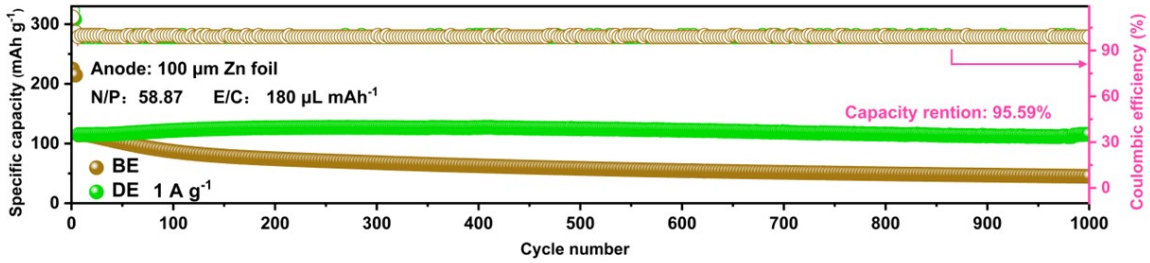

Figure S36. Long-term stabilities of the Zn/V_2O_5 full cells in BE and DE at 1 A g^{-1} under normal lab-scale test conditions of excessive Zn supply (100 μm Zn, N/P=58.87), flooded electrolyte (180 μLmAh^{-1}), and small cathode loading (0.99 mAh cm^{-2}), all the Zn/V_2O_5 cells were pre-activated at 0.1 A g^{-1} for five cycles.

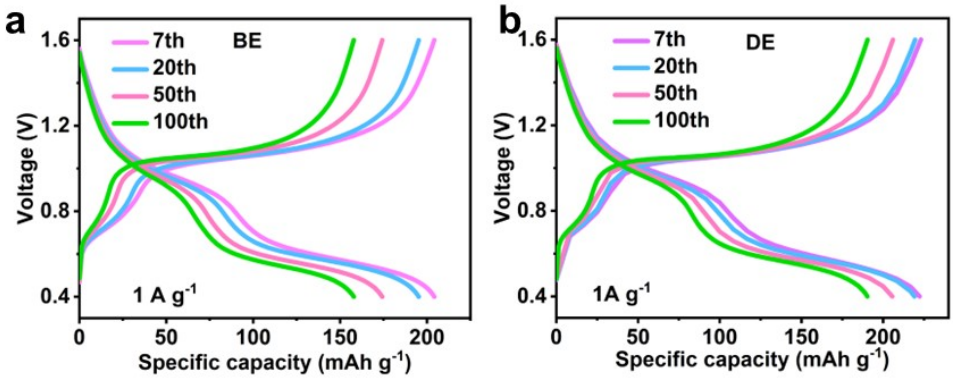

Figure S37. The corresponding voltage-capacity profiles of the Zn/V_2O_5 cells in (a) BE and (b) DE at 1 A g^{-1} under normal lab-scale test conditions.

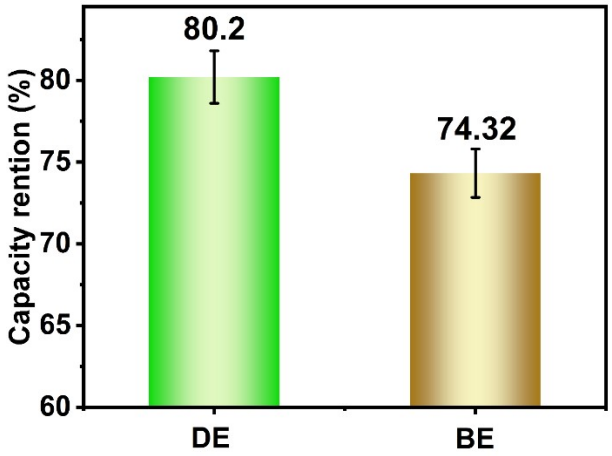

Figure S38. Capacity retention of the Zn/V_2O_5 full cells after self-discharge experiment. The error bars were obtained by parallel experiments for at least 3 times.

Table S1. The elemental composition corresponding to the EDS mapping (Figure 1b) of Zn foil after cycling in DE. The emergence of Si is observed on Zn surface after cycling in electrolyte with TEOS additive, indicating the formation of the protective film on Zn electrode and suppression of $(Zn(OH)_2)_3(ZnSO_4)(H_2O)_5$ formation.

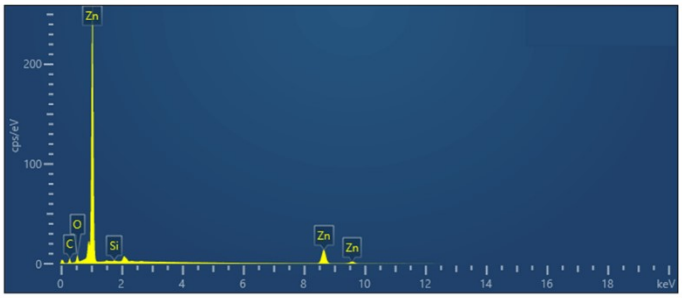

Element	Wt%	At%
C	13.14	42.18
O	3.48	8.38
Si	0.31	0.43
Zn	83.07	49.01

Table S2. The O–H stretching vibration fitted results of Raman spectra of the water molecules in BE, 20 mM DE, and 50 mM DE, respectively.

Electrolyte	Strong H-bond%	Weak H-bond%	None H-bond%
BE	42%	36%	22%
20 mM DE	32%	44%	24%
50 mM DE	21%	53%	26%

Table S3. Fitting results of the corrosion potential, corrosion density and corrosion current density of the Zn anode using BE or DE.

Electrolyte	E_{corr} (V)	I_{corr} (μA)	J_{corr} (μA cm^{-2})
BE	0.985	79.2	316.8
DE	0.983	28.6	114.4

Table S4. Fitting results of the EIS of the Zn|Zn symmetric cells using BE or DE.

Electrolyte	**BE**	**DE**
	R_s (Ω)	**R_s (Ω)**
Before cycling	192.0	331.0
After cycling	681.3	401.1

Table S5. The corresponding fitting results of the EIS of the Zn|Zn symmetric cells using BE or DE at different temperatures.

Electrolyte	**BE**		**DE**	
T (K)	**R_{ct} (Ω)**	**ln (R_{ct}^{-1}) ($Ω^{-1}$)**	**R_{ct} (Ω)**	**ln (R_{ct}^{-1}) ($Ω^{-1}$)**
293.15	1621.0	-7.39	822.1	-6.71
303.15	1355.0	-7.21	551.6	-6.31
313.15	919.0	-6.82	307.9	-5.72
323.15	469.0	-6.15	176.2	-5.17
333.15	266.5	-5.59	154.5	-5.04
343.15	144.3	-4.97	115.3	-4.75

Table S6. The corresponding fitting results of the EIS of the Zn/V_2O_5 full cells in BE and DE.

Electrolyte	**BE**	**DE**
R_1(Ω)	5.8	1.7
R_2(Ω)	335.1	82.8
R_3(Ω)	52.7	34.0

Table S7. Comparison of the electrochemical performance of Zn|Zn symmetric cells using DE with recently reported works on electrolyte engineering.

Electrolyte	Current density (mA cm^{-2})	Capacity (mAh cm^{-2})	Cycle life (h)	Cumulative capacity (mAh cm^{-2})	Ref.
TEOS/$ZnSO_4$	5	1	1264	3160	This work
1 M $ZnSO_4$+ 10 mM glucose	1	1	2000	1000	[1]
5 M $ZnCl_2$+ 5 M BT	0.5	0.5	1400	700	[2]
2 M $ZnSO_4$+ 2 mM SeO_2	2	2	2100	2100	[3]
2 M $ZnSO_4$+ 5 mg ml^{-1} silk sericin	10	5	400	2000	[4]
2 M $ZnSO_4$ + 10 vol.% DMA	1	1	400	200	[5]
3 M $ZnSO_4$ + 0.01 M TH	1	1	580	290	[6]
2 M $ZnSO_4$ + 8.5 M La $(NO_3)_3$	1	1	1200	600	[7]
LMS+ZSO	2.5	1.5	400	500	[8]
2 M $ZnSO_4$ + 10 mM Cys	0.5	0.5	2300	575	[9]
3 M $ZnSO_4$+ 10 mM a-CD	1	1	1000	500	[10]
2M $ZnSO_4$+20 mM CH_3COONH_4	2	1	2400	1200	[11]
2 M $Zn(OTf)_2$ + 0.2 M $ZnSO_4$	10	5	300	1500	[12]
3 M $Zn(OTf)_2$-(H_2O-HAc)+ TMS	5	5	300	750	[13]
2 M $ZnSO_4$+ 10 vol.% NMP	5	5	195	487.5	[14]

Table S8. Comparison of the deep-cycling performance of Zn|Zn symmetric cells using DE with recently reported Zn metal anodes with electrolyte engineering.

Electrolyte	Current density (mA cm^{-2})	Capacity (mAh cm^{-2})	Cycle life (h)	thickness	DOD (%)	Ref
TEOS/$ZnSO_4$	**1**	**46.5**	**830**	**100 μm**	**80**	**This work**
$Zn(BF_4)_2$/TMP	5	5	320	20 μm	42.7	[15]
a-CD/$ZnSO_4$	5	5	200	25 μm	30	[10]
BA/$ZnSO_4$	5	5	140	20 μm	38.1	[16]
SA/$ZnSO_4$	30	30	180	100 μm	64	[17]
glycerol/$ZnSO_4$	1	3	450	9 μm	51	[18]
AN/$ZnSO_4$	2	2	650	7 μm	50	[19]
$ZnSO_4$/$Zn(OTF)_2$	10	5	300	50 μm	17.1	[12]
$La(NO_3)_3$/$ZnSO_4$	10	5.93	160	12 μm	80	[7]
CO_2/$ZnSO_4$	10	10	100	30 μm	57	[20]

References

[1] P. Sun, L. Ma, W. Zhou, M. Qiu, Z. Wang, D. Chao, W. Mai, Angew Chem Int Ed Engl, 2021, **60**, 18247-18255.

[2] Z. Jia, W. Zhao, S. Hu, X. Yang, T. He, X. Sun, Chem Commun (Camb), 2022, **58(61)**: 8504-8507.

[3] C. Huang, X. Zhao, Y. Hao, Y. Yang, Y. Qian, G. Chang, Y. Zhang, Q. Tang, A. Hu, X. Chen, Advanced Functional Mater., 2022, 2112091.

[4] B. Wang, R. Zheng, W. Yang, X. Han, C. Hou, Q. Zhang, Y. Li, K. Li, H. Wang, Adv. Funct. Mater., 2022, **32(23)**.

[5] W. Deng, Z. Xu, X. Wang, Energy Storage Mater., 2022, **52**: 52-60.

[6] Z. Miao, Q. Liu, W. Wei, X. Zhao, M. Du, H. Li, F. Zhang, M. Hao, Z. Cui, Y. Sang, X. Wang, H. Liu, S. Wang, Nano Energy, 2022, **97.**

[7] R. Zhao, H. Wang, H. Du, Y. Yang, Z. Gao, L. Qie, Y. Huang, Nat. Commun., 2022, **13**.

[8] J. Cao, D. Zhang, Y. Yue, R. Chanajaree, S. Wang, J. Han, X. Zhang, J. Qin, Y. Huang, Nano Energy, 2022, **93**.

[9] Q. Meng, R. Zhao, P. Cao, Q. Bai, J. Tang, G. Liu, X. Zhou, J. Yang, Chem. Eng. J., 2022, **447.**

[10] K. Zhao, G. Fan, J. Liu, F. Liu, J. Li, X. Zhou, Y. Ni, M. Yu, Y. M. Zhang, H. Su, Q. Liu, F. Cheng, J Am Chem Soc, 2022, **144(25)**: 11129-11137.

[11] C. Lin, X. Yang, P. Xiong, H. Lin, L. He, Q. Yao, M. Wei, Q. Qian, Q. Chen, L. Zeng, Adv Sci (Weinh), 2022, e2201433.

[12] W. Yuan, G. Ma, X. Nie, Y. Wang, S. Di, L. Wang, J. Wang, S. Shen, N. Zhang, Chem Eng J, 2022, **431**, 134076.

[13] X. Zhao, X. Zhang, N. Dong, M. Yan, F. Zhang, K. Mochizuki, H. Pan, Small, 2022, **18**, e2200742.

[14] T. C. Li, Y. Lim, X. L. Li, S. Luo, C. Lin, D. Fang, S. Xia, Y. Wang, H. Y. Yang, Adv. Energy Mater., 2022.

[15] G. Ma, S. Di, Y. Wang, W. Yuan, X. Ji, K. Qiu, M. Liu, X. Nie, N. Zhang, Energy Storage Mater., 2023, **54**, 276-283.

[16] B. Liu, C. Wei, Z. Zhu, Y. Fang, Z. Bian, X. Lei, Y. Zhou, C. Tang, Y. Qian, G. Wang, Angew Chem Int Ed Engl, 2022, **144(25)**: 11129-11137.

[17] C. Huang, F. Huang, X. Zhao, Y. Hao, Y. Yang, Y. Qian, G. Chang, Y. Zhang, Q. Tang, A. Hu, X. Chen, Adv. Funct. Mater., 2022, 2210197

[18] Y. J. Zhang, M. Zhu, K. Wu, F. F. Yu, G. Y. Wang, G. Xu, M. H. Wu, H. K. Liu, S. X. Dou, C. Wu, J. Mater. Chem., A 2021, **9**, 4253-4261.

[19] [Z. Hou, H. Tan, Y. Gao, M. H. Li, Z. H. Lu, B. Zhang, J. Mater. Chem., A 2020, **8**, 19367-19374.

[20] Y. Zhu, H. Y. Hoh, S. Qian, C. Sun, Z. Wu, Z. Huang, L. Wang, M. Batmunkh, C. Lai, S. Zhang, Y. L. Zhong, ACS Nano, 2022, **16(9)**: 14600-14610.